Biol Cybern (2007) 97:81–97
DOI 10.1007/s00422-007-0155-3

ORIGINAL PAPER

Biological Cybernetics

Kinetic models of spike-timing dependent plasticity and their functional consequences in detecting correlations

Quan Zou · Alain Destexhe

Received: 17 November 2006 / Accepted: 30 March 2007 / Published online: 25 May 2007

Abstract Spike-timing dependent plasticity (STDP) is a type of synaptic modification found relatively recently, but the underlying biophysical mechanisms are still unclear. Several models of STDP have been proposed, and differ by their implementation, and in particular how synaptic weights saturate to their minimal and maximal values. We analyze here kinetic models of transmitter-receptor interaction and derive a series of STDP models. In general, such kinetic models predict progressive saturation of the weights. Various forms can be obtained depending on the hypotheses made in the kinetic model, and these include a simple linear dependence on the value of the weight ("soft bounds"), mixed soft and abrupt saturation ("hard bound"), or more complex forms. We analyze in more detail simple soft-bound models of Hebbian and anti-Hebbian STDPs, in which nonlinear spike interactions (triplets) are taken into account. We show that Hebbian STDPs can be used to selectively potentiate synapses that are correlated in time, while anti-Hebbian STDPs depress correlated synapses, despite the presence of nonlinear spike interactions. This correlation detection enables neurons to develop a selectivity to correlated inputs. We also examine different versions of kinetics-based STDP models and compare their sensitivity to correlations. We conclude that kinetic models generally predict soft-bound dynamics, and that such models seem ideal for detecting correlations among large numbers of inputs.

Keywords STDP · Synaptic plasticity · Computational models · Biophysical models

Q. Zou · A. Destexhe (✉)
Integrative and Computational Neuroscience Unit (UNIC), CNRS,
1 Avenue de la Terrasse, 91198 Gif-sur-Yvette, France
e-mail: Destexhe@iaf.cnrs-gif.fr

1 Introduction

Over the past years, growing experimental evidence has demonstrated that both the amplitude and the direction of synaptic plasticity can depend on the precise timing of presynaptic and post-synaptic action potentials (Levy and Steward 1983; Debanne et al. 1994; Bell et al. 1997; Markram et al. 1997; Magee and Johnston 1997; Bi and Poo 1998), a form of synaptic modification, which is termed *spike-timing dependent plasticity* (STDP). This type of plasticity was demonstrated by using dual recordings of connected neurons and using stimulation protocols in which the excitatory postsynaptic potential (EPSP) arising from presynaptic cell's firing is coupled with postsynaptically elicited spikes at different latencies. Typically, potentiation is observed when the EPSP precedes the postsynaptic spike, whereas the reversed temporal order induces depression of the EPSP. Such a "Hebbian" STDP with similar characteristics was observed in neocortical slices (Markram et al. 1997), hippocampal slices (Magee and Johnston 1997) and cell cultures (Bi and Poo 1998), whereas the opposite temporal window ("anti-Hebbian") was observed in the electrosensory lobe of the electric fish (Bell et al. 1997).

Computational models of STDP were proposed both at the biophysical (Castellani et al. 2001; Senn et al. 2001; Shouval et al. 2002; Karmarkar and Buonomano 2002; Abarbanel et al. 2003; Badoual et al. 2006; Rubin et al. 2005; Shouval and Kalantzis 2005) and phenomenological levels (Gerstner et al. 1996; Kistler and van Hemmen 2000; Song et al. 2000; van Rossum et al. 2000; Rubin et al. 2001; Gerstner and Kistler 2002; Karbowski and Ermentrout 2002; Gütig et al. 2003; Badoual et al. 2006; Pfister and Gerstner 2006). Biophysical models attempt to find plausible biophysical or biochemical pathways to account for STDP, while phenomenological models provide algorithmic rules that account for

the dynamics of STDP without necessarily trying to explain them. An advantage of biophysical models is that they can also account for more complex paradigms of interaction between pairs of pre- and post-synaptic spikes, such as the frequency-dependence of STDP (Sjöström et al., 2001) or nonlinear interactions between successive pairs (Froemke and Dan 2002), which can emerge from biophysical models (Badoual et al. 2006).

Generally, phenomenological models can be implemented either additively (Song et al. 2000; Gütig et al. 2003; Badoual et al. 2006) or multiplicatively (van Rossum et al. 2000; see also discussion in Gerstner and Kistler 2002). However, treating the interaction between multiple pairs of spikes either way makes no qualitative difference (Izhikevich and Desai 2003). In other words, it does not matter whether each pairing changes the conductance by a percentage of its existing value or by a fixed amount. What does matter is the boundary of the updating rules. For example, in Song and Abbott's model of STDP, the synaptic weight is artificially clipped to minimal and maximal values. Such "hard bounds" retain inherently unstable dynamics while exhibiting strong competition between afferent synapses. The synaptic weights are driven to the bounds, which leads to a bimodal distribution (Song et al. 2000). This model has been used, for example, to account for cortical remapping during development (Song and Abbott 2001).

In contrast, the dynamics of synaptic weights can saturate progressively to its boundaries. Such "soft bound" models (Kistler and van Hemmen 2000; van Rossum et al. 2000; Rubin et al. 2001; Gütig et al. 2003; Badoual et al. 2006; Morrison et al. 2007), generate a stable, unimodal distribution of synaptic weights with reduced competition, while both potentiation and depression attenuate as the corresponding upper or lower boundary is approached (van Rossum et al. 2000). A model generalizing soft and hard bounds was proposed by Gütig et al. (2003), by using an ad-hoc scaling of the weight dependence of evolution equations. This model can be switched between unimodal or bimodal weight distributions. Finally, a model was proposed based on a power-law dependence of synaptic weights, which is also consistent with experimental data (Morrison et al. 2007).

In this paper, we explore kinetic models of STDP based on either presynaptic or postsynaptic changes. We consider simple kinetic schemes for the changes in weight, triggered by either pre- or post-synaptic mechanisms. We investigate which type of dynamics (soft-bound or hard-bound) emerges, and to what extent the models obtained are consistent with the available experimental data. We next analyze the behavior of one of those models in detail, and in particular, with respect to processing correlated inputs. We terminate by a comparison of the different STDP rules identified in kinetic models with respect to their ability to detect correlations.

2 Methods

Kinetic models of transmitter-receptor interaction were based on previous models of synaptic transmission and post-synaptic receptors (Destexhe et al. 1994, 1998). STDP will be integrated in such models, as shown in Results. Several kinetic models of STDP will be proposed, and several of these kinetic models will be investigated numerically. We detail below the methods used in these different steps.

2.1 Soft-bound and hard-bound models of STDP

The equation describing the time evolution of the synaptic weight ω for a synapse with soft bounds can be written as:

$$\frac{d\omega}{dt} = -F_{LTP}(t)\,(\omega-\omega_{LTP}) - F_{LTD}(t)\,(\omega-\omega_{LTD}), \quad (1)$$

where ω_{LTP} and ω_{LTD} are respectively the maximal and minimal values of the synaptic weight. In this type of model, the weight is necessarily bounded between ω_{LTP} and ω_{LTD} and the saturation to these values is "soft", in the sense that the derivative of the weight is attenuated linearly as it approaches its bounds. Similar models were introduced before (Kistler and van Hemmen 2000; van Rossum et al. 2000; Rubin et al. 2001; Gütig et al. 2003; Badoual et al. 2006). The functions $F_{LTP}(t)$ and $F_{LTD}(t)$ describe the interaction between pre- and post-synaptic activity and will be described below.

Similarly, one can define the time evolution of the synaptic weight ω for a synapse with "hard bounds":

$$\frac{d\omega}{dt} = \left[F_{LTP}(t) - F_{LTD}(t)\right]_{\omega_{LTD}}^{\omega_{LTP}}, \quad (2)$$

where the operator $[\ldots]_{\omega_{LTD}}^{\omega_{LTP}}$ represents a clipping of the synaptic weight so that it is bounded between ω_{LTP} and ω_{LTD} ("hard bounds"). In this case, there is no modulation of the amount of change as a function of the value of the weight. This model is similar to Song et al. (2000).

2.2 Interaction between pre- and post-synaptic spikes

$F_{LTP}(t)$ and $F_{LTD}(t)$ are functions describing the coincidence between pre- and post-synaptic spikes. When the pre/post spike timing should lead to long-term potentiation (LTP), $F_{LTP}(t) > 0$ and $F_{LTD}(t) = 0$; conversely, for long-term depression (LTD), $F_{LTP}(t) = 0$ and $F_{LTD}(t) > 0$. These functions are zero otherwise. As in a previous model (Badoual et al. 2006), these functions are given by:

$$F_{LTP} = \sum_{t_i,t_j} P(t-t_j)\,\delta(t-t_i) \quad (3)$$

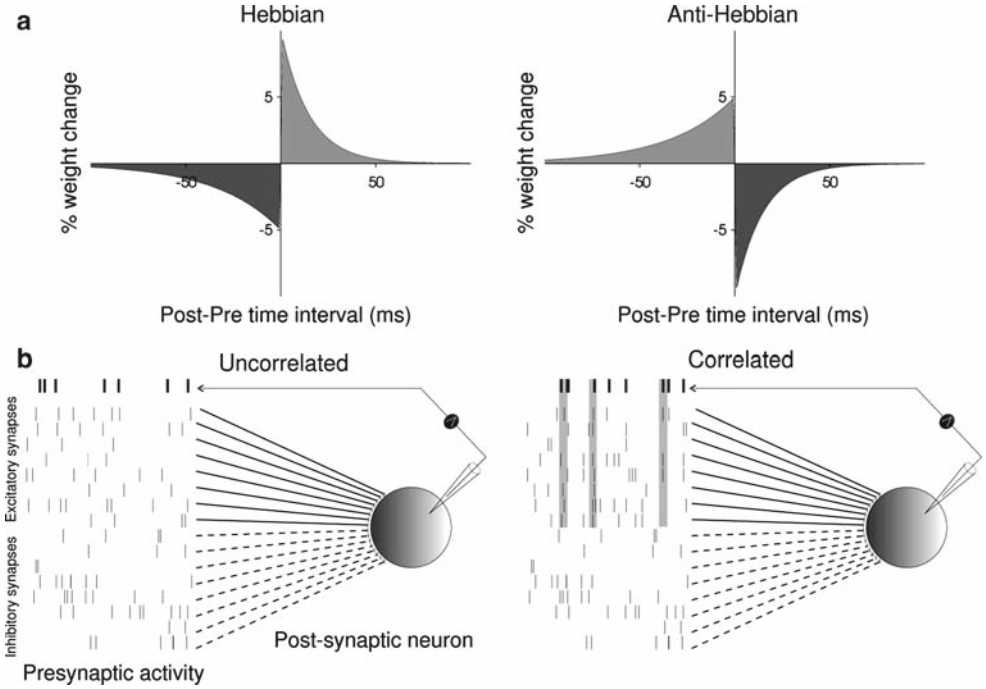

Fig. 1 Scheme of the plasticity windows and correlations used in the model. **a** Hebbian and anti-Hebbian STDP functions. The percentage change of the peak conductance at a synapse following paired pre- and post-synaptic spikes is plotted as a function of Δt, the time of the post-synaptic spike minus the time of the pre-synaptic spike. The STDP function is shown for the classic Hebbian rule (*left*), as well as for anti-Hebbian STDP (*right*). **b** Illustration of the correlation paradigms used in the model. A model neuron was submitted to excitatory and inhibitory synapses, releasing randomly according to Poisson processes. The synaptic release events (indicated here by *vertical bars*) could be either uncorrelated (*left*) or correlated (*right*). In the case of correlated release, the release frequency was unchanged at individual synapses, but the probability of co-releasing (*gray shades* in the right diagram) was increased. The postsynaptic activity (*dashed box*) may show correlations with presynaptic activity

$$F_{\mathrm{LTD}} = \sum_{t_i,t_j} Q(t-t_i)\,\delta(t-t_j)\,, \tag{4}$$

where t_j and t_i are the times of pre- and post-synaptic spikes, respectively, and the sums run over all possible pairs of pre- and post-synaptic spikes. $P(t) = A_p \exp(-t/\tau_p)$ and $Q(t) = A_q \exp[-(t)/\tau_q]$ define the time window of interaction between spikes ($\tau_{\mathrm{p}} = 14.8$ ms, $\tau_{\mathrm{q}} = 33.8$ ms, $\mathrm{A_p} = 0.1$, and $\mathrm{A_q} = 0.05$). These functions define the "STDP function" represented in Fig. 1a.

The model investigated numerically incorporates a very important property of STDP identified recently: multiple pairs of spikes do not interact linearly but follow a nonlinear rule. This was demonstrated by experiments using spike triplets (Froemke and Dan 2002). The same study also showed that such nonlinear spike interactions can be accounted for by introducing "spike eligibility" factors (Froemke and Dan 2002). Including such effects in the soft-bound STDP model leads to the following set of equations:

$$\frac{\mathrm{d}\omega_{ji}}{\mathrm{d}t} = -\epsilon_i\,\epsilon_j\left[F_{\mathrm{LTP}}(t)\,(\omega_{ji}-\omega_{\mathrm{LTP}}) + F_{\mathrm{LTD}}(t)\,(\omega_{ji}-\omega_{\mathrm{LTD}})\right], \tag{5}$$

where ϵ_i and ϵ_j are spike eligibility factors given by:

$$\epsilon_i = 1-\exp\left[-\left(\frac{t-t_i^{\mathrm{last}}(t)}{\tau_s^{\mathrm{post}}}\right)\right],$$

$$\epsilon_j = 1-\exp\left[-\left(\frac{t-t_j^{\mathrm{last}}(t)}{\tau_s^{\mathrm{pre}}}\right)\right],$$

where $\tau_s^{\mathrm{pre}} = 28$ ms, $\tau_s^{\mathrm{post}} = 88$ ms and t_k^{last} gives the time of the last spike in neuron k (Froemke and Dan 2002).

Equations 5 constitute the main model investigated numerically, and they were integrated using an optimized algorithm described in Appendix 1. Note that these equations use accelerated weight changes for convenience. The simulations were checked with 10 times slower changes, which led to slower convergence but the steady-state weight distributions were unchanged (see Results).

2.3 Neuron model

To investigate the properties of STDP, we simulated single compartment models that included voltage-dependent

conductances described by Hodgkin and Huxley (1952) type kinetics:

$$
\begin{aligned}
C_{\mathrm{m}}\,\frac{\mathrm{d}V}{\mathrm{d}t} &= -g_{\mathrm{leak}}(V-E_{\mathrm{leak}}) - I_{\mathrm{Na}} - I_{\mathrm{Kd}} - I_{\mathrm{M}} - I_{\mathrm{syn}} \\
I_{\mathrm{Na}} &= \overline{g}_{\mathrm{Na}}\, m^3 h\, (V-E_{\mathrm{Na}}) \\
I_{\mathrm{Kd}} &= \overline{g}_{\mathrm{Kd}}\, n^4\, (V-E_{\mathrm{K}}) \\
I_{\mathrm{M}} &= \overline{g}_{\mathrm{M}}\, p\, (V-E_{\mathrm{K}}),
\end{aligned}
\tag{6}
$$

where $C_m = 1\ \mu F/cm^2$ is the specific membrane capacitance, $\overline{g}_{leak} = 0.045$ mS/cm^2 is the leak conductance density, and $E_{leak} = -80$ mV is the leak reversal potential. I_{Na} is the voltage-dependent Na^+ current and I_{Kd} is the 'delayed-rectifier' K^+ current responsible for action potentials. I_M is a non-inactivating K^+ current responsible for spike frequency adaption. These currents and parameter settings were the same as in a biophysical model cortical regular-spiking cell (Destexhe and Paré 1999; Destexhe et al. 2001).

Synaptic currents were simulated by two-state kinetic models of glutamatergic (AMPA) and GABAergic ($GABA_A$) receptor types (Destexhe et al. 1994, 1998):

$$
I_{\mathrm{syn}_{ji}} = \omega_{ji}\, m\, (V - E_{\mathrm{syn}})\,, \tag{7}
$$

where ω_{ji} is the synaptic weight as above (which also plays the role of the maximal conductance), m is the fraction of postsynaptic receptors in the open state (see below), V is the postsynaptic membrane potential, and $E_{syn}$is the reversal potential of the synaptic current.

The fraction of activated receptors m is calculated according to a simple two-state model of transmitter/receptor interaction:

$$
R_u + T \underset{\beta}{\overset{\alpha}{\rightleftharpoons}} R_b\,, \tag{8}
$$

where R_u and R_b are the unbound and bound receptor forms, respectively, T is the transmitter, while α and β are rate constants. The corresponding kinetic equation for this system is:

$$
\frac{\mathrm{d}m}{\mathrm{d}t} = \alpha\,[T]\,(1-m) - \beta\, m\,, \tag{9}
$$

where $[T]$ is the concentration of transmitter in the synaptic cleft. We assume that the transmitter concentration occurs as a pulse of 1 ms and 1 mM amplitude, and we use standard parameters to describe AMPA and $GABA_A$ receptors (Destexhe et al. 1998). Quantal conductances were of 25 nS for AMPA and 10 nS for $GABA_A$. $\alpha = 0.94$ ms^{-1}mM^{-1} and $\beta = 0.18$ ms^{-1} for AMPA, $\alpha = 10.5$ ms^{-1}mM^{-1} and $\beta = 0.166$ ms^{-1} for $GABA_A$. Metabotropic and N-methyl-D-aspartate (NMDA) receptors were not included.

2.4 Generating and detecting correlations

Both excitatory and inhibitory synapses were driven by Poisson-distributed random spike trains. In some simulations, a correlation between some pre-synaptic spike trains was introduced, as illustrated in Fig. 1b. To generate correlated pre-synaptic spike trains, a set of N_2 independent Poisson-distributed random variables was generated and distributed randomly among the N pre-synaptic trains. Every time step the Poisson trains were redistributed. Correlation arose from the fact that $N_2 \leq N$ and the ensuing redundancy within the N pre-synaptic trains (Destexhe and Paré 1999).

To calculate cross-correlations between two spike trains x(i) and y(i), we used *Pearson's correlation*:

$$
r(d) = \frac{\sum_i [\,(x(i)-\bar{x})\,(y(i+d)-\bar{y})\,]}{\sqrt{\sum_i (x(i)-\bar{x})^2}\sqrt{\sum_i (y(i)-\bar{y})^2}}, \tag{10}
$$

where $\bar{x}$ and $\bar{y}$ are the mean spike numbers of the corresponding spike trains and d is a time-delay. The denominator normalizes the correlation coefficient such that $-1 \leq r(d) \leq 1$. The correlation values obtained were in the range 0.005 to 0.05, as found experimentally in awake monkeys (Zohary et al. 1994).

2.5 High-conductance state

To simulate the intense synaptic activity similar to in vivo conditions (Destexhe et al. 2003), we considered AMPA and GABAergic synapses with the same density (1 synapse per 200 μm^2 of membrane): 190 synapses for total 38013.27 μm^2 membrane area (Destexhe and Paré 1999), low and high-conductance states were generated by different conditions of release for GABAergic and glutamatergic synapses. The release conditions corresponding to in vivo–like activity were estimated based on a series of intracellular recordings during active states (Destexhe and Paré 1999; Paré et al. 1998; Steriade et al. 2001). From these measurements, the relative ratio of contribution of excitatory and inhibitory conductances during high-conductance states were estimated: $\langle g_{i0}\rangle/\langle g_{e0}\rangle$, is between 4 and 5. (reviewed by Destexhe et al. 2003). Assuming that synaptic conductances and release properties are uniform and described by Poisson processes, we found that the constraints above led to estimates of the average release frequency during active states, which was about 2.4 and 3.2 Hz for glutamatergic and GABAergic synapses, respectively (these particular values were taken from a previous estimate based on intracellular recordings in anesthetized rats; see Zou et al.). These input rates were used in all simulations throughout the paper, unless explicitly stated.

We also tested the model in low-conductance states defined by lower release conditions. However, in this case simu-

lations took considerably longer time because less spikes were produced (sometimes leading to complete silence). In high-conductance states, the activity of the neurons can be maintained more robustly and avoid this drawback.

All simulations and analyses were performed in the NEURON simulation environment (Hines and Carnevale 1997) under the LINUX operating system.

3 Results

We start by analyzing kinetic models of synaptic transmission and STDP, and in which case they lead to hard- or soft-bound dynamics. We then analyze numerically and analytically such models and emphasize the role of correlations in affecting synaptic weights, differentially for Hebbian or anti-Hebbian STDPs.

3.1 Kinetic models of STDP

The pre-synaptic or post-synaptic localization of changes underlying synaptic plasticity is a subject of intense investigation and debate (for recent reviews, see Anwyl 2006; Dan and Poo 2006; Duguid and Sjostrom 2006; Nicoll 2003; Soderling and Derkach 2000). Here, we successively consider pre- and post-synaptic mechanisms for plasticity, in the framework of simple kinetic models of transmitter/receptor interaction, and how this affects the hard- or soft-bound character of the dynamics.

3.1.1 Postsynaptic models of STDP

We first investigate a purely postsynaptic model of STDP, in which synaptic changes solely depend on the regulation of postsynaptic receptors. We consider a simple model of the regulation kinetics of postsynaptic receptors, which main assumption is that synaptic strength depends on the number of "active" postsynaptic receptors, and that there are activity-dependent mechanisms to activate or inactivate these receptors. Active and inactive forms may represent the phosphorylated and dephosphorylated forms of AMPA receptors identified experimentally (reviewed in Roche et al. 1994; Wang et al. 2005). Calling R_1 the inactive form, and R^* the active form of the receptor, one can write the synaptic weight ω as:

$$\omega \;=\; \bar{\omega}\,(r_0 + r^*)\;, \tag{11}$$

where $\bar{\omega}$ is the maximal weight of the synapse (if all receptors were in active form), and r^* is the fraction of receptors in active form R^*. r_0 is the fraction of receptors in a "stable" form (i.e., non activable or inactivable), which gives a minimal strength of the synapse (this factor is included for convenience and has no effect on the following, besides imposing a non-zero lower bound).

According to a simple first-order mechanism, the regulation of receptors from inactive to active form, and vice-versa, obeys the kinetic equation:

$$R_1 \underset{F_{\mathrm{LTD}}(t)}{\overset{F_{\mathrm{LTP}}(t)}{\rightleftharpoons}} R^*\;, \tag{12}$$

where the rate functions $\mathrm{F_{LTP}}(t)$ and $\mathrm{F_{LTD}}(t)$ are function of time as well as pre- and post-synaptic activities (see below). According to the choice of the functions $\mathrm{F_{LTP}}(t)$ and $\mathrm{F_{LTD}}(t)$, one can implement any STDP learning rule.

Using the relation $r_1 = 1 - r^* - r_0$, one can write Equation 12 as:

$$\frac{\mathrm{d}r^*}{\mathrm{d}t} \;=\; F_{\mathrm{LTP}}(t)\;(1 - r^* - r_0) \;-\; F_{\mathrm{LTD}}(t)\;r^*\;. \tag{13}$$

Using relation (11), the synaptic weight evolves according to:

$$\frac{\mathrm{d}\omega}{\mathrm{d}t} \;=\; -\;F_{\mathrm{LTP}}(t)\;(\omega - \bar{\omega}) \;-\; F_{\mathrm{LTD}}(t)\;(\omega - \bar{\omega} r_0)\;. \tag{14}$$

Thus, by identifying $\omega_{\mathrm{LTP}} = \bar{\omega}$ and $\omega_{\mathrm{LTD}} = \bar{\omega}\,r_0$, this equation is identical to Eq. 1. The soft bounds of this model come from the fact that the resources (the total number of available receptors) are necessarily limited. Note that the above results are valid for any model of transmitter/receptor interaction and receptor kinetics, provided the postsynaptic receptors exist in active and inactive forms (Eq. 12). We also tested more complex versions of this equation with more states and obtained qualitatively the same results (not shown).

3.1.2 Experimentally measurable synaptic weights

To link the above model of STDP to experimentally measurable parameters, we take Eq. 7 for the synaptic current at synapse ij, $I_{\mathrm{syn}_{ji}}$, together with the simplest model of transmitter/receptor interaction (two-state open/close scheme as in Eqs. 8 and 9). According to this scheme, if the pulse of transmitter T is of duration T_{dur} and amplitude T_{max}, the maximum of the fraction of open receptors m during an isolated synaptic current is given by:

$$m_{\mathrm{peak}} \;=\; 1 - \mathrm{e}^{-\alpha\;T_{\mathrm{max}}\;T_{\mathrm{dur}}}\;. \tag{15}$$

Thus, because the peak synaptic conductance is given by:

$$g_{\mathrm{peak}} \;=\; \omega_{ji}\;\left[1 - \mathrm{e}^{-\alpha\;T_{\mathrm{max}}\;T_{\mathrm{dur}}}\right]\;, \tag{16}$$

the soft bound dynamics of the synaptic weight ω_{ji} will linearly translate into the dynamics of the peak conductance. As the peak of synaptic conductance is probably the best

measure of synaptic weight,[1] we conclude that this type of postsynaptic model necessarily implies soft bounds for synaptic weights.

3.1.3 Presynaptic models of STDP

To check whether other mechanisms can give models with hard bounds, similar to the Song et al. (2000) model, one must consider alternative biologically-plausible mechanisms. The most obvious alternative to the postsynaptic model above is a purely presynaptic model, where the amount of postsynaptic receptors is fixed, but the quantity of transmitter (or equivalently its peak concentration) varies. In this case, one can see that from Eq. 7 that this is equivalent to assume that the maximal conductance of the synapse (ω_{ji}) is bounded (by the fixed amount of receptors), whereas the fraction of receptors in the open state (m) is allowed to be modulated by STDP (instead of following stereotyped dynamics as above). If we take the same model of transmitter/receptor interaction as above, but allow the amplitude of the transmitter concentration in the cleft, $T_{\max}$ to vary (but that in the context of a single release event, $T_{\max}$ remains constant, so that we still have a pulse of transmitter), then the relations derived above apply, in particular the peak conductance is given by:

$$g_{\text{peak}} = g_{\max}\left[1 - \mathrm{e}^{-\alpha\, T_{ji}\, T_{\text{dur}}}\right] . \tag{17}$$

Here, we have replaced the previous dynamic term ω_{ji} by a constant term $g_{\max}$, and the previous constant term $T_{\max}$ by T_{ji}, which is allowed to vary according to STDP.

Comparing this situation with the previous postsynaptic model (Eq. 16), we can see that there is no longer a linear dependence between the variables undergoing STDP and the peak synaptic conductance. If the synapse becomes maximally depressed, g_{peak} tends to zero as expected, but if the transmitter concentration reaches arbitrarily high values, the value of the postsynaptic conductance will be necessarily bounded by $g_{\max}$. So even if the "output" of the presynaptic compartment, the amount of transmitter released, is not bounded, the synaptic conductance will be necessarily bounded by the constraints of the kinetics of postsynaptic receptors. Thus, in the framework of the assumptions made above, any model of either pre- or post-synaptic plasticity will necessarily be bounded.

The question of whether these bounds are "hard" or "soft" can be approached by studying how synaptic weights vary in time. Starting from Eq. 17, we can derive the time derivative of the peak synaptic conductance:

$$\frac{\mathrm{d}g_{\text{peak}}}{\mathrm{d}t} = \alpha\, T_{\text{dur}}\, g_{\max}\, \mathrm{e}^{-\alpha\, T_{ji}\, T_{\text{dur}}}\, \frac{\mathrm{d}T_{ji}}{\mathrm{d}t} , \tag{18}$$

which, by using the relation $g_{\max}\, \mathrm{e}^{-\alpha\, T_{ji}\, T_{\text{dur}}} = (g_{\max} - g_{\text{peak}})$, simplifies to:

$$\frac{\mathrm{d}g_{\text{peak}}}{\mathrm{d}t} = \alpha\, T_{\text{dur}}\, (g_{\max} - g_{\text{peak}})\, \frac{\mathrm{d}T_{ji}}{\mathrm{d}t} . \tag{19}$$

Assuming a hard-bound rule for the transmitter concentration, similar to Eq. 2 yields

$$\frac{\mathrm{d}T_{ji}}{\mathrm{d}t} = \Big[F_{\text{LTP}}(t) - F_{\text{LTD}}(t)\Big]_{T_{\text{LTD}}}^{T_{\text{LTP}}} , \tag{20}$$

where $\mathrm{T_{LTP}}$ and $\mathrm{T_{LTD}}$ are the "hard" bounds of transmitter concentration. Combining with Eq. 19 gives

$$\frac{\mathrm{d}g_{\text{peak}}}{\mathrm{d}t} = \alpha\, T_{\text{dur}}\, (g_{\max} - g_{\text{peak}}) \times \Big[F_{\text{LTP}}(t) - F_{\text{LTD}}(t)\Big]_{T_{\text{LTD}}}^{T_{\text{LTP}}} . \tag{21}$$

Here, we can easily recognize a similar functional form as for soft bound models (compare with Eq. 1). The first term ($\mathrm{F_{LTP}}(t)$) will drive the peak conductance towards the maximal value $g_{\max}$, similar to the drive towards ω_{LTP} in Eq. 1. In contrast, the second term ($\mathrm{F_{LTD}}(t)$) will drive g_{peak} down, and this drive may appear as unbounded. It is bounded, however, because T must remain positive by definition ($\mathrm{T_{LTD}} \geq 0$), so by Eq. 20, the hard bound to the derivative of T must necessarily ensure that g_{peak} always remains positive.

Thus, in the case of presynaptic models, the peak conductance will not vary according to a hard-bound model, even if presynaptic release is subject to hard-bound STDP. The peak conductance is saturating softly to its maximal value, whereas its minimal value is hard bounded. If we assume a soft-bound presynaptic rule for $T_{\max}$, then the peak synaptic conductance will obey a more complex form of soft-bounded dynamics. Note that for all models tested, the only way to obtain hard bounds was to assume that some variable of the model is itself hard-bounded (such as in Eq. 20), but we were unable to find any plausible biophysical or kinetic mechanism naturally leading to hard-bound dynamics.

3.1.4 Are experimental data consistent with hard-bound or soft-bound STDP?

Before turning to numerical simulations, we discuss the consistency of the above considerations with experiments. Experimental data have shown that the relative weight increase (defined as the weight increase divided by the initial weight) varies nonlinearly with initial weight (Bi and Poo 1998; see also Montgomery et al. 2001 for LTP). The authors typically represent the relative weight change as a function of the logarithm of initial weight, ω_0. However, the type of nonlinearity observed will be highly dependent on the type of model considered, so we investigated this issue here for kinetic models of STDP.

[1] Another measure of synaptic weight is the integral of synaptic conductance, but it is proportional to the peak value, because the the synaptic current decays exponentially.

For hard-bound models, the change of weight will be independent on the initial value ω_0:

$$\omega - \omega_0 \;=\; C\,, \tag{22}$$

where C is a constant (positive for LTP, negative for LTD). The relative weight change is then given by:

$$(\omega - \omega_0)/\omega_0 \;=\; C/\omega_0\,. \tag{23}$$

Such a behavior is represented in Fig. 2a, where the $1/\omega_0$ dependence in Eq. 23 gives rise to a decreasing exponential dependence as a function of $\log(\omega_0)$.

In soft-bound models, integrating the generic equation

$$\frac{\mathrm{d}\omega}{\mathrm{d}t} \;=\; (\omega_S - \omega_0)\; F(t)\,, \tag{24}$$

where ω_S is the steady-state value of the weight, leads to:

$$\omega - \omega_0 \;=\; A\;(\omega_S - \omega_0)\,, \tag{25}$$

where $A > 0$ is a constant. The relative weight change is given by

$$(\omega - \omega_0)/\omega_0 \;=\; A\;(\omega_S - \omega_0)/\omega_0\,. \tag{26}$$

Thus, for soft-bound models, the relative weight change will also be an exponential function of $\log(\omega_0)$, as shown in Fig. 2b. A particular case is for LTD, if $\omega_S = 0$, the relative weight change becomes independent of ω_0 and equals $-A$ (Fig. 2b, LTD, solid line). If the steady-state weight ω_S for LTD is non-zero, a small nonlinearity appears (Fig. 2b, LTD, dashed line)

Experimental data (see Fig. 5 of Bi and Poo 1998) show that the relative weight change indeed decreases nonlinearly with initial weight for LTP (see also Montgomery et al. 2001). However, in this logarithmic representation, it is not possible to distinguish between hard- and soft-bound models. For LTD, the data seem more consistent with soft-bound models with $\omega_S = 0$ (see also van Rossum et al. 2000; Morrison et al. 2007). To unambiguously distinguish between the two type of models, it is preferable (when experimentally possible) to use the absolute weight change, $\omega - \omega_0$, and represent it against initial weight ω_0, as shown in Fig. 2c. For hard-bound models, the weight change is independent of ω_0 (dotted lines in Fig. 2c) while for soft-bound models, this representation will reveal the type of weight dependency, which is linear in the type of model considered here (see Fig. 2c, solid lines).

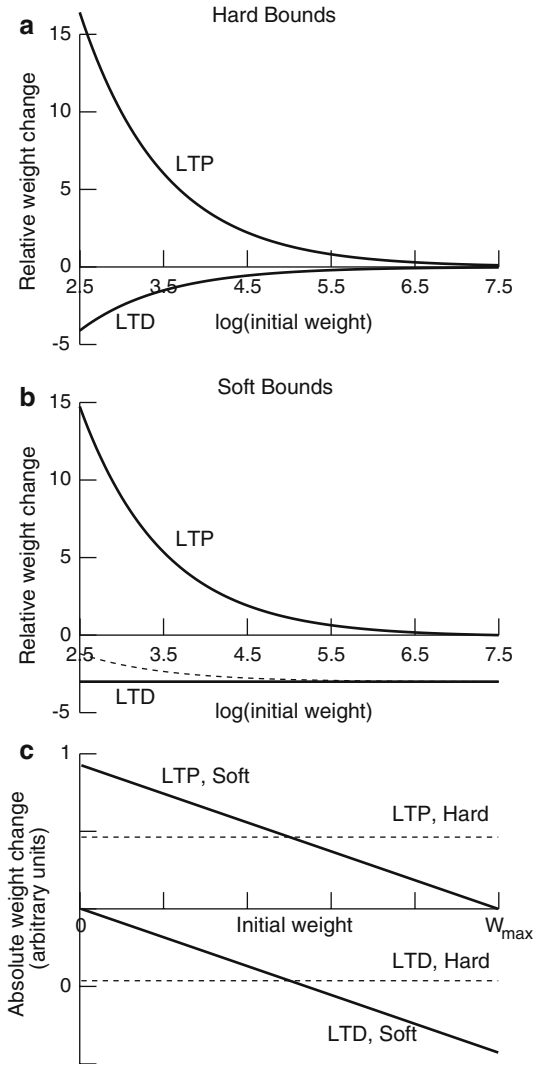

Fig. 2 Weight-dependence of kinetic models of STDP. **a** Relative weight change represented as a function of the logarithm of initial weight for a hard-bound model of STDP (Eq. 23 with $C = 200$ for LTP and $C = -50$ for LTD). **b** Same representation for a soft-bound model of STDP (Eq. 26) with $A = 3$ and $\log(\omega_S)$=7.5 for LTP and for LTD: $\log(\omega_S)$=-1000 (*solid line*) and $\log(\omega_S)$=2 (*dashed line*). **c** Representation of the absolute weight change $(\omega - \omega_0)$ as a function of initial weight (ω_0) for the two type of models (*dashed lines* for hard-bound model, *solid lines* for soft-bound model). The hard-bound models plotted the expression $\omega - \omega_0 = A(\omega_S - \omega_0)$ with $\omega_S = W_{\max}$ for LTP and $\omega_S = 0$ for LTD

3.2 Behavior of the soft bound model of STDP

We now turn to numerical investigations of the soft-bound model of STDP by using a Hodgkin–Huxley type model driven by conductance-based synapses subject to STDP (see Methods). The synaptic weight change as a function of the delay between pre- and post-synaptic spikes is shown in Fig. 1a for Hebbian (left panel) and anti-Hebbian STDP (right panel). This function will be called here *STDP function* for simplicity, and was modeled by two exponentials (see Methods), similar to previous studies (Song et al. 2000; van Rossum et al. 2000; Gütig et al. 2003). The decay time constant of the exponentials determines the extent of the temporal window in which STDP operates. Following experimental measurements (Bi and Poo 1998; Froemke and Dan 2002), we let $\tau_p = 14.8$ ms, and $\tau_q = 33.8$ ms for Hebbian plasticity (Fig. 1a, left). The temporal asymmetry of the synaptic

modification is represented by the opposite signs of weight changes for positive and negative time differences. The anti-Hebbian plasticity rule is obtained by simply reversing the signs of weight changes for Δt (Fig. 1a, right), but keeping the decay time constants unchanged.[2]

In this numerical investigation, we consider nonlinear spike interactions (triplets) through the use of spike-eligibility factors (Froemke and Dan 2002; see Sect. 2). Previous models emphasized the sensitivity of STDP to correlations (Song et al. 2000; van Rossum et al. 2000; Gütig et al. 2003) but did not incorporate such nonlinear interactions. We investigate here the correlation sensitivity of soft-bound STDP models endowed with nonlinear spike interactions (see Eq. 5 in Sect. 2).

3.2.1 Distributions of synaptic weights

We first investigated the steady-state distribution of synaptic weights in this soft-bound model of STDP. We simulated a Hodgkin–Huxley neuron receiving random (Poisson-distributed) synaptic inputs at AMPA and $GABA_A$ synapses (see Methods). Synaptic weights were initially distributed randomly between the two extreme values ω_{LTD} (which was zero unless otherwise stated) and ω_{LTP}. As time evolves, synaptic weights converge towards a stable steady-state distribution due to soft-bound STDP dynamics.[3] This distribution is unimodal, consistent with previous observations with soft-bound STDP models (van Rossum et al. 2000; Rubin et al. 2001; Gütig et al. 2003). The extent and position of the weight distribution depends on the different parameters of the model. One of those parameters is the integral of the STDP function, as shown in Fig. 3. For Hebbian STDP, the steady-state weight distribution converged to large values of weights if the positive lobe (potentiation) was prominent (Fig. 3a,c), which corresponds to a small ratio $A_q\tau_q/A_p\tau_p$. Conversely, if the integral tends to be negative (depression lobe dominant), the distribution tends to smaller values of weights. A similar behavior was also found for anti-Hebbian STDP models (not shown).

To explain these observations, we first define the *mean steady-state synaptic weight*, $\langle g \rangle$, as the mean value of the steady-state weight distribution. To better understand how the exact shape of the STDP function affects this parameter, we constructed surrogate postsynaptic spike trains by randomly reshuffling postsynaptic spikes, thereby completely decorrelating them with the pre-synaptic AMPA inputs. In this case, the STDP operates between two uncorrelated (pre- and post-synaptic) random trains of spikes. A similar dependency as described above was still present (Fig. 3b,c). In such a case, the mean synaptic weight could be predicted by using the

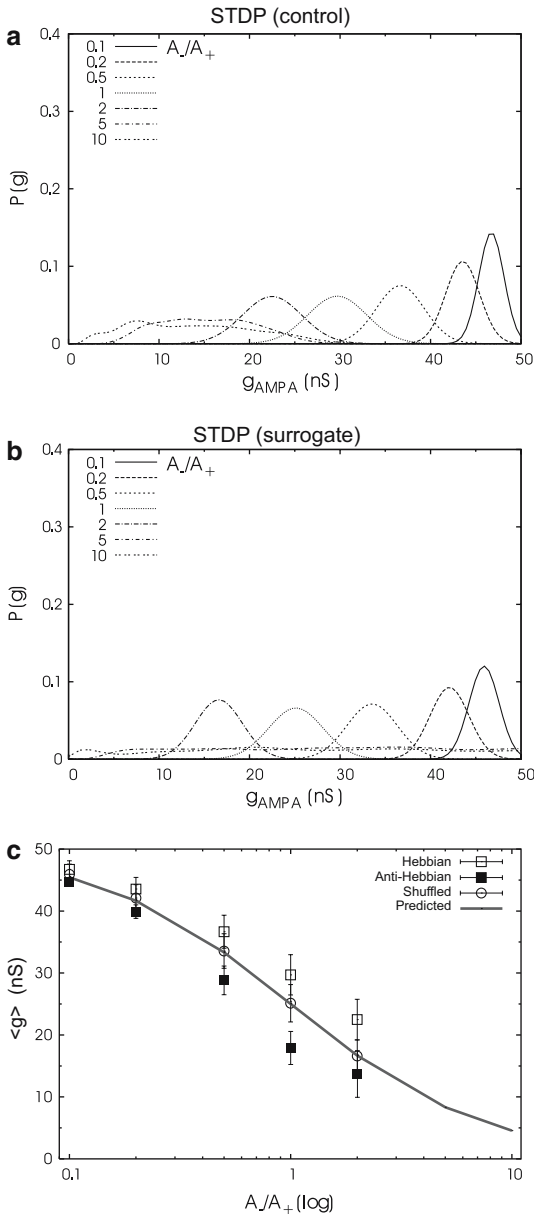

Fig. 3 Unimodal distributions of synaptic weights in a soft-bound kinetic model of STDP. The steady-state distribution of synaptic weights is shown for different parameters of the STDP function. The release rates at synapses were fixed (γ_{AMPA}=2.4 Hz, γ_{GABA}=3.2 Hz), but different values of A_-/A_+ were used (see legend in inset). **a** Steady-state distributions obtained in a model neuron using soft-bound Hebbian STDP models. **b** Distribution obtained in the same model, but when pre- and post-synaptic spikes were decorrelated by reshuffling post-synaptic spikes (surrogate analysis). **c** Mean of the steady-state distribution of synaptic weights, $\langle g \rangle$, for different conditions (see legend), plotted as a function of the value of A_-/A_+ in log scale. The prediction was obtained from Eq. 27. All simulations were run over 3,600 s, and the distribution was sampled from the last 600 s, to make sure the equilibrium was reached

[2] Note that the anti-Hebbian STDP is not simply the inverse of the Hebbian STDP because of the inclusion of nonlinear spike interactions.

[3] It must be noted that only the weight distribution is reaching steady-state, while individual synaptic weights continue to vary.

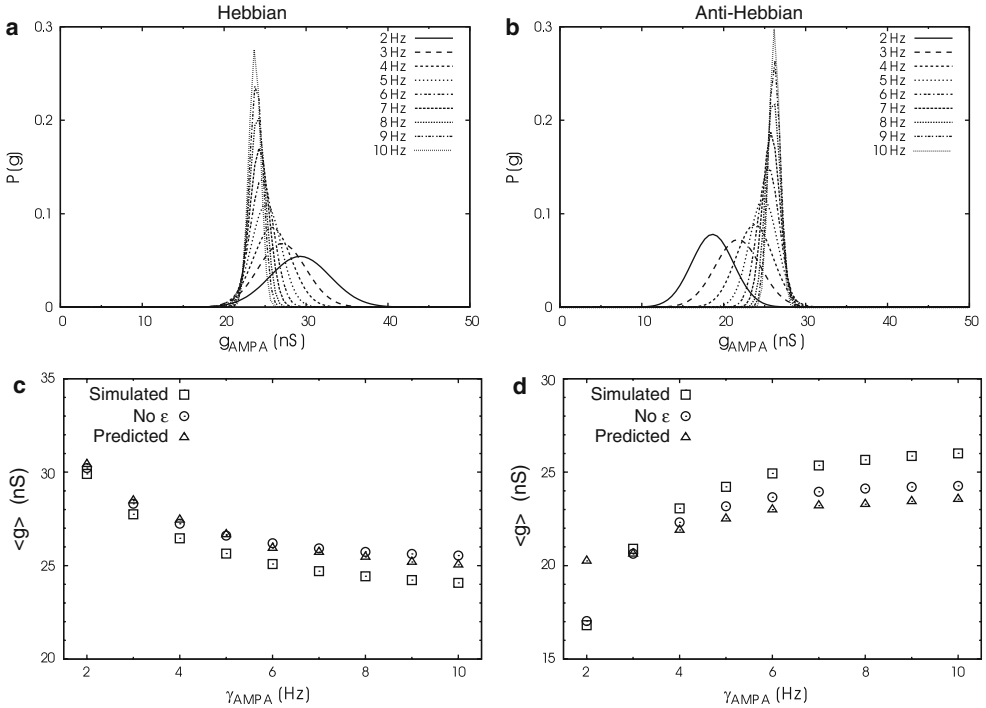

Fig. 4 Effect of the release rate on the distribution of synaptic weights. **a** Effect of release rate on the steady-state distribution of synaptic weights for Hebbian STDP with uncorrelated random inputs. **b** Same set of simulations for anti-Hebbian STDP. **c** Mean synaptic weight (average value of the steady-state distribution) represented as a function of the rate. The data represented are from (**a**) ("Simulated", squares), and are compared to the analytic estimate ("Predicted", triangles) obtained from Eq. 28. The same simulations were also done without the spike eligibility factors ("No ϵ", circles). **d** Same representation as in (**c**), but for anti-Hebbian STDP (data from **b**)

following relation for the steady-state synaptic weight (see Appendix 2):

$$\langle g \rangle = \frac{\omega_{\mathrm{LTP}}}{1 + (A_-/A_+)}, \tag{27}$$

where $A_+ = \mathrm{A_p}\,\tau_\mathrm{p}$ and $A_- = \mathrm{A_q}\,\tau_\mathrm{q}$ are the positive and negative areas under the STDP function, respectively. The mean steady-state synaptic weight calculated numerically (Fig. 3c, circles) was well predicted by this analytic estimate (Fig. 3c, continuous line).[4]

We next used this surrogate analysis to directly appreciate the effect of causality between pre- and post-synaptic spikes. With Hebbian STDP on excitatory synapses, the mean weight was always larger than for the surrogate case (Fig. 3c, compare open squares with continuous line). On the other hand, anti-Hebbian plasticity gave rise to smaller mean weights (see Fig. 3c, filled squares). Another interesting difference is that the weight distribution remains almost flat for very low firing rates (Fig. 3b), showing that STDP is ineffective at modifying synapses when there are too few post-synaptic spikes, as noted earlier (Song et al. 2000). However, this was only the case for surrogate postsynaptic spikes, as the distributions for the same firing rates were significatively different in the control condition (Fig. 3a, leftmost distributions), while the other distributions were similar. Thus, the effect of causality between pre- and post-synaptic spikes is most prominent for low firing rates.

Similar results hold for GABAergic synapses (not shown), except that in this case, the dependency is opposite to that shown in Fig. 3c. Hebbian STDP on GABAergic synapses leads to mean weights that are lower than for surrogate postsynaptic spikes, while the anti-Hebbian STDP produces the opposite.

3.2.2 *Effect of release rates*

We next investigated the effect of the release rate at AMPA synapses by simulating a HH neuron model subject to random excitatory and inhibitory release events at different rates (Fig. 4). For Hebbian STDP, the mean synaptic weight decreases as the input rates increases (from 2 to 10 Hz; see Fig. 4a; Fig. 4c, squares). The opposite is seen for anti-Hebbian STDP (Fig. 4a; Fig. 4c, squares).

To explain this paradoxical effect (see also Song et al. 2000; Burkitt et al. 2004), we used the following relation

[4] Note that for some parameters ($A_-/A_+ = 5, 10$ in Fig. 3), depression is much larger than potentiation and the distributions are very broad, partly due to the fact that equilibrium was not reached because depression prevented postsynaptic spiking to drive synaptic weights to equilibrium.

to predict the mean synaptic weight (see Appendix 2 for details):

$$\langle g \rangle = \frac{\omega_{\mathrm{LTP}}}{1 + \frac{\int Q(\tau)\, C_{ij}(\tau)\, \mathrm{d}\tau}{\int P(\tau)\, C_{ji}(\tau)\, \mathrm{d}\tau}}, \tag{28}$$

where $C_{ij}(\tau)$ and $C_{ji}(\tau)$ are cross-correlations between pre- and post-synaptic spikes. $C_{ij}(\tau)$ is proportional to the probability that a pre-synaptic spike occurs at a time delay τ after a post-synaptic spike, and inversely, $C_{ji}(\tau)$ is related to the probability that a post-synaptic spike occurs at a time delay τ after a pre-synaptic spike. Thus, the mean synaptic weight depends on the integral of the STDP function and the cross-correlations between pre- and post-synaptic activities (a similar relation was obtained in another model (Gütig et al. 2003). Note that large values of the mean weight can still be obtained when cross-correlation values are very small, because it is given by the ratio of these values integrated—see Eq. 28. These cross-correlations can easily be calculated from the model for different release rates (Fig. 5a). Using this expression led to a good prediction of the mean weight obtained by numeric simulations (Fig. 4c; compare circles with triangles). Note that we performed this prediction by running the model with $\epsilon_i = \epsilon_j = 1$ in Eq. 5 (in agreement with the assumptions of Eq. 28; see Appendix 2), but both models had the same trend.

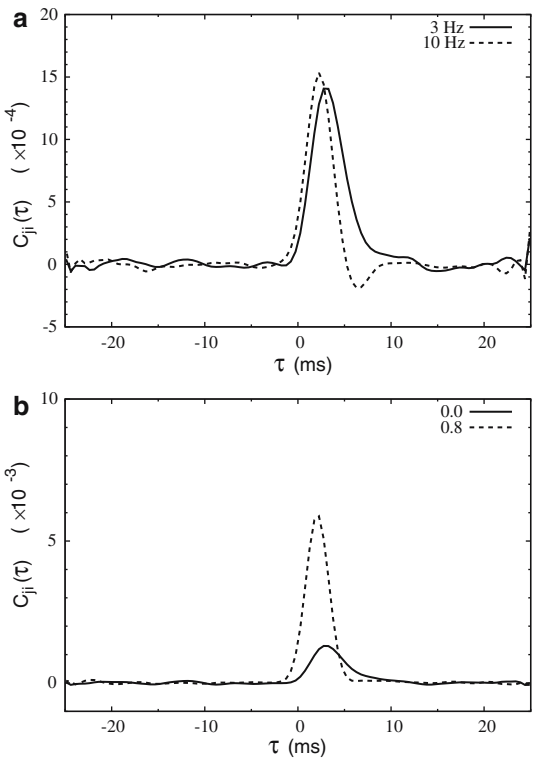

Fig. 5 Cross-correlation between pre- and post-synaptic spikes. **a** Cross-correlation between pre- and post-synaptic activity ($C_{ji}(\tau)$), represented as a function of the time delay (τ) for the model of Hebbian STDP at two release rates (3 Hz, *solid line*; 10 Hz *dashed line*; same simulations as in Fig. 4a,c). **b** Same representation for two different values of the correlation index (0=uncorrelated, *solid line*; 0.8=highly correlated presynaptic activity, *dashed line*; same simulations as in Fig. 6a,c)

Thus, this effect of the decrease of the mean steady-state weight with increasing rates can be explained by examining the cross-correlations in Fig. 5a. The correlation function is narrower with higher release rates, presumably because the neuron reaches threshold faster with higher-frequency inputs.[5] It is straightforward to see that integrating those functions with the STDP functions will lead to a lower steady-state values for higher rates.

3.2.3 *Effect of correlations*

We next investigated the effect of introducing correlations between release events (see Sect. 2). In contrast with the effect of release rate, the mean steady-state synaptic weight increased as the correlation coefficient increased from 0 to 0.8 (Fig. 6a; Fig. 6c, squares). The opposite behavior was observed for anti-Hebbian STDP models (Fig. 6b; Fig. 6d, squares). Computing cross-correlations (Fig. 5b) and using Eq. 28 to predict the mean weight led to a reasonably good agreement between simulated and predicted values (Fig. 6c-d; note that the errors for anti-Hebbian STDP models is due to poor statistics because of low firing rates in this case). We also found that the postsynaptic firing rate followed the value of the pre-synaptic correlation (not shown), although the total number of inputs did not change (the release rate was constant). This is consistent with previous findings (Rudolph and Destexhe 2001) showing that pre-synaptic correlations are very efficiently detected by neurons. When synapses were endowed with STDP, this correlation detection was even more prominent. The opposite effect on postsynaptic firing rate was observed for anti-Hebbian STDP (not shown).

3.2.4 *Correlation processing*

The above results show that the soft-bound STDP model endowed with nonlinear spike interactions can reliably detect correlations, consistent with previous models which did not include this nonlinearity (van Rossum et al. 2000; Gütig et al. 2003). This correlation sensitivity was also present when only a subset of synapses were correlated. In this case, only this specific subset of synapses was potentiated (for Hebbian STDP) or depressed (for anti-Hebbian STDP; not shown).

To further test the ability to process correlations, we simulated a paradigm in which the correlation was dynami-

[5] Note that this is not due to a conductance effect, because simulating the same model with current-based inputs led to nearly identical results (not shown).

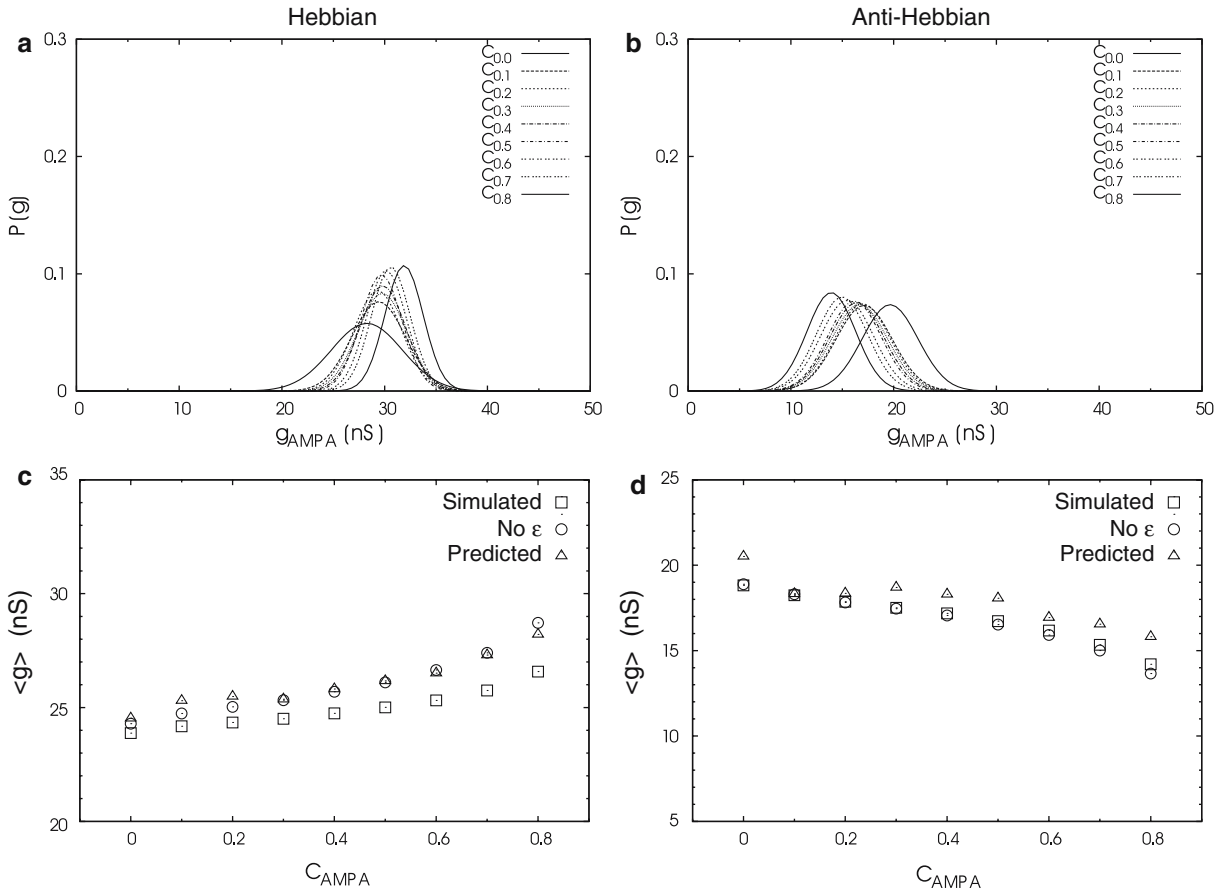

Fig. 6 Effect of presynaptic correlations on the distribution of synaptic weights. **a** Effect of correlations on the steady-state distribution of synaptic weights for Hebbian STDP. Excitatory and inhibitory input rates were fixed at 2.4 and 3.2 Hz, respectively. **b** Same representation for anti-Hebbian STDP models. **c** Mean synaptic weight represented as a function of the value of the correlation index ("Simulated", *squares*; data from **a**), compared to the analytic estimate ("Predicted", *triangles*; Eq. 28). The same simulations were also done without the spike eligibility factors ("No ϵ", *circles*). **d** Same representation as in **c** for anti-Hebbian STDP models (data from **b**)

cally changed within different groups of synapses. As shown in Fig. 7a, two group of synapses were simulated with different correlations, leading to convergence of the weights to two sets of values. At a given time (first arrow in Fig. 7a), the correlations were switched between the two groups. As expected, this induced relaxation of the weights to a new equilibrium state corresponding to the new values of correlations. At a further time (second arrow in Fig. 7a), the correlations were switched back to the initial values, again leading to relaxation towards steady-state.[6] Interestingly, these dynamic changes in synapses occurred with no change in mean firing rate (Fig. 7, right panel). A similar paradigm also applies to inhibitory synapses, in which case the changes in weight are opposite (Fig. 7b). Anti-Hebbian STDP models also gave opposite changes as Hebbian STDP models (not shown).

We next investigated the effect of STDP on "correlation transfer" between pre-synaptic neurons and post-synaptic neurons. If presynaptic neurons become correlated, they could drive the firing of the postsynaptic neuron, such that this neuron also becomes correlated with the presynaptic population of correlated neurons, and in some sense becomes "recruited" into the assembly of correlated neurons. Since STDP is sensitive to correlations, it could be a good candidate to realize such a recruitment. We tested this idea by calculating the "output" correlation between postsynaptic spikes and presynaptic trains ("post-pre correlation"), and comparing it to the "input" correlation between presynaptic trains ("pre-pre correlation"). Without STDP, the output correlation was increasing as a function of the input correlation (Fig. 8a, circles), while the time to peak decreased (not shown). Hebbian STDP reinforced these relations (Fig. 8a, squares), while anti-Hebbian STDP weakened it (Fig. 8a, triangles). An effect of correlations was also present if the

[6] Slight differences in kinetics appear between the two transitions in Fig. 7a, the relaxation to upper values is faster than to lower values. This is presumably attributable to the asymmetry of the STDP function. Inverse results were obtained using anti-Hebbian STDP, with faster relaxation to lower values (not shown).

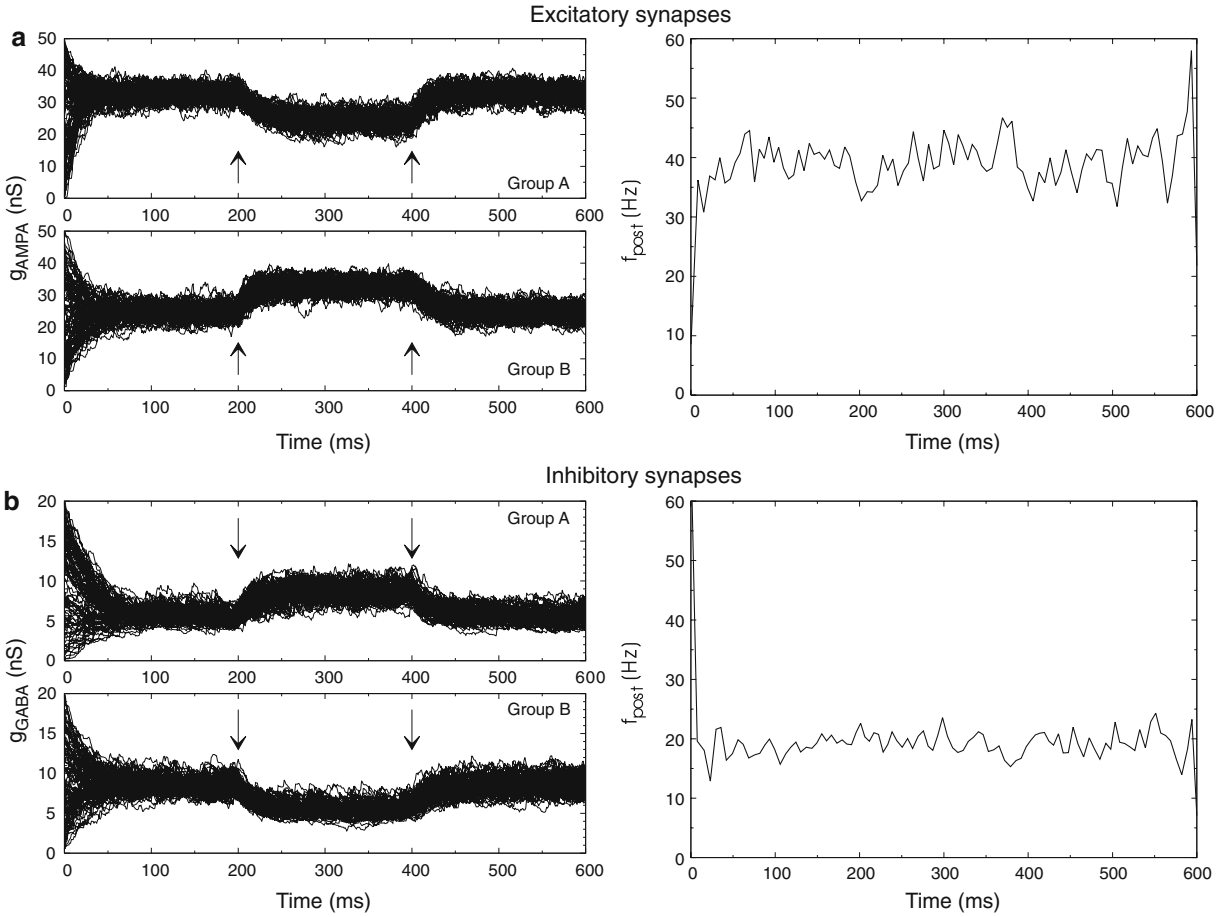

Fig. 7 Dynamic changes in correlation can modify synapses with no change in mean firing rate. **a** Correlation alternation within two subsets of excitatory synapses (50% each). Initially, Group A was correlated at 0.5, while Group B was non-correlated. The neuron converged to a steady firing rate (*right panel*). At $t = 200\ ms$, the correlation was switched between the two groups, leading to a decrease of the synaptic weights in group A and an increase for group B (*left panel, first arrow*). 200 ms later, the correlation was switched back to initial values (*second arrow*). **b** Same paradigm for GABAergic synapses. Hebbian STDP was used in all cases

same paradigm was applied to inhibitory synapses (Fig. 8b), but there was no significant effect of plasticity in this case. In all cases, however, the output correlation remained smaller in magnitude compared to the input correlation, and this was independent on the total number of synapses simulated (Fig. 8c) or maximal weight (Fig. 8d).

Finally, we compared the correlation sensitivity of different STDP rules, some of which were predicted by kinetic models. Figure 9 shows a comparison of the effect of correlation on weight distributions for different combinations of hard- and soft-bounds for LTP and LTD, in the presence of nonlinear spike interactions. As seen above, correlations affect the weight distribution for the soft-bound model of STDP (Fig. 9a). Correlations also affect a mixed model with hard-LTD combined with soft-LTP (Fig. 9b), which model was predicted when changes occur presynaptically and assuming presynaptic hard bounds. The mirror situation, with soft-LTD and hard-LTP is also sensitive to correlations, which tend to saturate the weight towards their maximal value (Fig. 9c). The hard-bound model of STDP, similar to Song et al. (2000), is only weakly sensitive to correlations (Fig. 9d). In contrast, the hard-bound model was reported to be sensitive to correlations (Song et al. 2000). We indeed observed this sensitivity, but only if nonlinear spike interactions were not included by setting $\epsilon_i = 1$ (not shown). Thus, we conclude that the weak sensitivity of hard-bound STDP to correlations is due here to the presence of nonlinear spike interactions.

4 Discussion

In this paper, we have analyzed simple kinetic models of STDP and found that postsynaptic changes predict soft-bound dynamics because of the resources (such as the number of receptors) are necessary limited. The situation is, however, different for presynaptic models, which do not lead to such clear-cut conclusion. If the amount of transmitter released is assumed to obey hard bounds, the rate of change

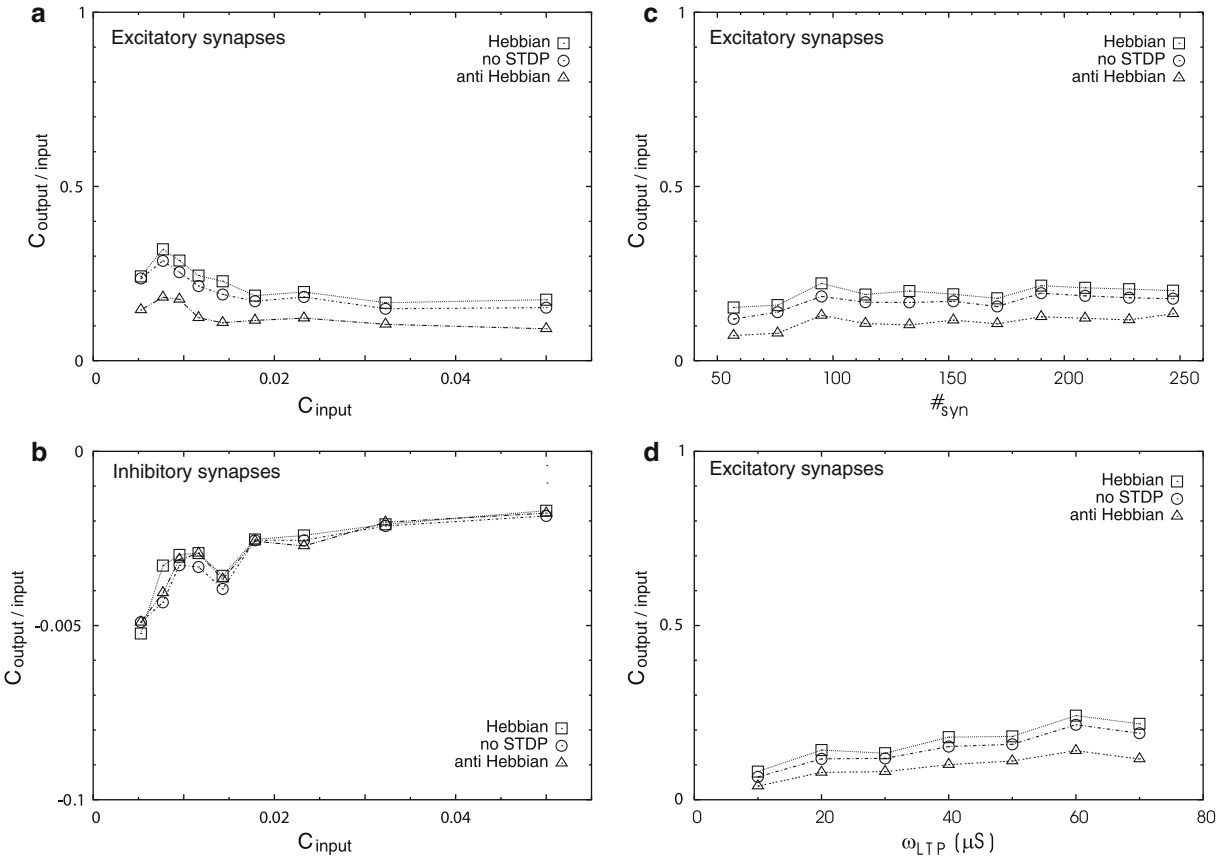

Fig. 8 Correlation transfer from pre-synaptic neurons to post-synaptic neuron during STDP. Model neuron receiving 190 glutamatergic and GABAergic synapses. The Pearson cross-correlation was calculated either between presynaptic and postsynaptic spike trains ("output correlation") or within presynaptic trains ("input correlation", C_{input}), and the ratio between these two values ($C_{output/input}$) was represented for various conditions. **a** Correlation transfer for STDP at excitatory synapses (maximal conductance g_{AMPA} = 25 nS, rate of 2.4 Hz; inhibitory synapses fixed at 10 nS, rate of 3.2 Hz). The different curves show the ratio of cross-correlations ($C_{output/input}$) for Hebbian STDP (*squares*), no STDP (*circles*) and anti-Hebbian STDP (*triangles*) at excitatory synapses, as a function of input correlation (C_{input}). **b** Similar protocol of simulations, but when inhibitory synapses were subject to STDP. **c** Same simulations as in (**a**), but $C_{output/input}$ is represented as a function of the number of excitatory synapses (ranging from 57 to 247), while releasing at a rate which was scaled such that the total effective synaptic conductance was unchanged. The input correlation was kept to similar values for each set of synapses (Pearson correlation included between 0.014 and 0.021). D. Same simulation as in (**a**) for different maximal values of excitatory synaptic weight (ω_{LTP}). The input correlation was in this case fixed at 0.018

of the synaptic conductance will be a mixture of hard and soft bounds, with soft upper bound and hard lower bound. Such a rule was, to our knowledge, never tested and constitutes one interesting prediction of such kinetic models worth being explored in more detail in future work.

We next performed a series of numerical simulations to explore these models of STDP, with emphasis to explain their dynamics. The main originality of this numerical investigation is that the simulated models incorporated the nonlinear spike interactions identified experimentally (Froemke and Dan 2002). For soft-bound models, we found that a critical parameter is the total area under the STDP function. The STDP functions used here (Fig. 1a) were fit to a biophysical model and to different experimental measurements (see details in Badoual et al. 2006), which gave the result that the integral of the STDP function was negative for Hebbian STDP and positive for anti-Hebbian STDP (Fig. 1a). A negative integral requires $A_q \tau_q > A_p \tau_p$, which is an important assumption in Song et al. model: the synaptic weakening through STDP is, overall, slightly larger than synaptic strengthening and this is a requisite for stability (Song et al. 2000). This requirement is relaxed for soft-bound STDP as there is no such instability, since the weights necessarily converge to a steady-state distribution comprised in between the two extreme values.

We also found a paradoxical effect that augmenting the release rate led to a decrease of the mean synaptic weight (see Fig. 4a,c), while the opposite holds for anti-Hebbian STDP models(Fig. 4b,d). This effect was also observed previously in STDP models (Song et al. 2000; Burkitt et al. 2004; but see Rubin et al. 2001), and is confirmed here in the presence of nonlinear spike interactions. This effect could

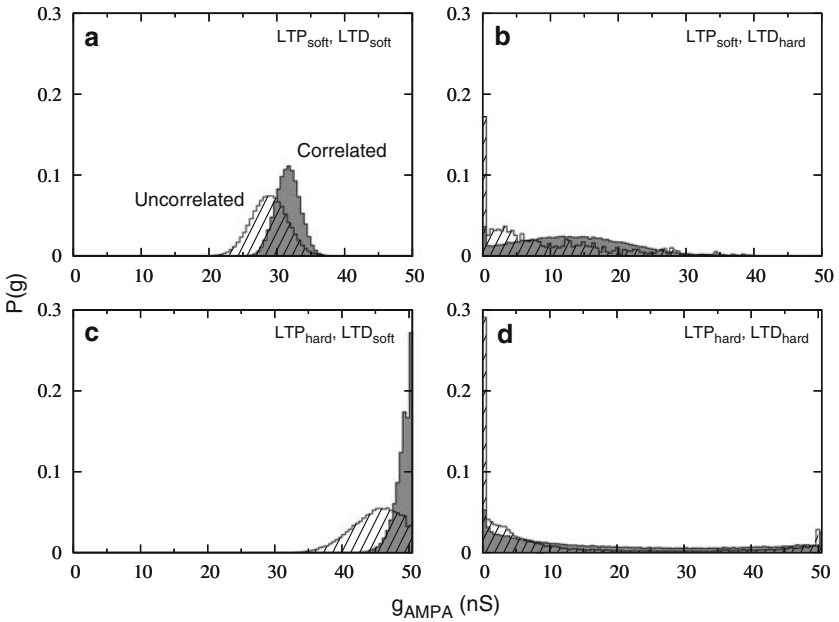

Fig. 9 Effect of correlations in the synaptic weight distribution for different STDP rules. The neuron model received 190 glutamatergic and GABAergic synapses with fixed releasing rate of 2.4 and 3.2 Hz, respectively. Each graph compares the distribution obtained with uncorrelated synaptic inputs (*black*) with that obtained when inputs were correlated (*gray*; Pearson correlation of 0.018). **a** Soft-bound model identical to that predicted by a postsynaptic kinetic model of STDP. **b** Soft-bounded LTP with hard-bounded LTD, as predicted by kinetic models when changes occur presynaptically. **c** Hard-bounded LTP with soft bounds for LTD. **d** Hard-bound model of STDP. In both (**b**) and (**c**), to achieve the balance of dynamic between potentiation and depression, the maximal modification of STDP curve ($A_p$and A_q) was scaled appropriately

be explained by the broadening of the cross-correlations for low rates, which leads to higher mean weights (the same can also be deduced from the analysis given in Gütig et al. 2003). Interestingly, this situation implements a type of homeostasis with respect to postsynaptic firing rate. For low input rates, the mean synaptic weight shifts to high values, which give large post-synaptic firing rates. Conversely, for high input rates, the mean synaptic tends to lower values, which in turn gives low post-synaptic firing rates. This indicates that Hebbian STDP could rescue the neuron firing at low input rates, but inhibits it at high input rates (and conversely for anti-Hebbian STDP).

The equation for the steady-state weight (Eq. 28) directly includes the cross-correlations between pre- and post-synaptic activities. If inputs are correlated, this cross-correlation increases dramatically (Fig. 5b) and the mean synaptic weight is thus directly affected by input correlations (Fig. 6). This effect of correlations is interesting, and is clearly due to the fact that correlated release events have more chance to fire the neuron (Rudolph and Destexhe 2001), and thus, to fulfill the condition for being potentiated (for Hebbian STDP) or depressed (for anti-Hebbian STDP). This is a good example of cooperativity between synapses, because at a given synapse, the statistical characteristics of the release pattern remains unchanged, but it is the respective timing of release events at different synapses which is effective in being detected by the STDP window, leading to changes in synaptic weight. Such changes would not have occurred for uncorrelated synapses releasing with the same characteristics.

This ability for STDP to "pick-up" timing information was further illustrated by including correlations only within subsets of inputs, and in this case, only the correlated subsets are subject to changes with STDP (not shown). This shows that STDP can very efficiently detect groups of correlated synaptic inputs and selectively potentiate (or depress) them. Such synaptic modifications can occur between different groups of synapses, without necessarily observing changes in the mean firing rate of the neuron (Fig. 7). Such correlation changes have been observed experimentally in various systems and such correlation changes are related to the behavior of the animal (Vaadia et al. 1995; de Charms and Merzenich 1996; Riehle et al. 1997).

In line with this potentially important role of correlation for representing information, we investigated how correlations can be processed and transmitted from pre- to post-synaptic activity. We found that STDP enhances the "output" correlation (Fig. 8), enabling the postsynaptic neuron to become correlated with those presynaptic neurons that were already correlated, and in a sense be recruited in the population of correlated cells. On the other hand, anti-Hebbian STDP will tend to opposite this effect by reducing the output correlation. These results suggest that groups of neurons

connected with excitatory synapses endowed with soft-bound STDP can easily form assemblies of correlated firing. Such formation of correlated assemblies is facilitated by Hebbian STDP, which is also in line with the original ideas of Hebb (Hebb 1949). This formation of assemblies is also consistent with the synfire chains concept (Abeles 1991). However, in the present case there is no strict synchronous firing, but the correlation is defined as occasional coincidences in the spiking of neurons (which is exactly what was simulated by our distributed correlation algorithm).

Finally, we compared different STDP rules, such as soft-bound, hard-bound, or mixed hard and soft bounds. We found that either soft-bound or mixed rules are able to detect correlations. The hard-bound STDP model, which was previously reported to be sensitive to correlations (Song et al. 2000), was only weakly sensitive when nonlinear spike interactions were taken into account. Interestingly, the two types of STDP dynamics predicted by kinetic models, soft-bound or mixed hard-soft bounds, are both efficient to detect correlations. We did not consider more complex cases, such as power-law dependence, as suggested recently (Morrison et al. 2007). The types of kinetic models of STDP that we considered here predict a simple dependence on synaptic weights, and even with nonlinear spike interactions, such models are entirely consistent with time-based computing paradigms based on temporal or spatial correlations.

Appendix 1: Integration algorithm

Since the algorithm must examine all possible pairs of pre- and post-synaptic spikes, one needs to optimize the calculations to avoid combinatorial explosion of spike pairs as time evolves. We used an iterative scheme, which we explain below for potentiation. This procedure is similar to that presented in Song et al. (2000), with the important difference that we take here the nonlinear spike interactions into account.

Potentiation is calculated at the time a post-synaptic spike occurs (t_i), and is theoretically a function of the pairs made with all pre-synaptic spikes (t_j^k) that occurred at time t_i. This amounts to calculate the following expression:

$$\sum_{k=0}^{m} P[t_i - t_j^k]\, \epsilon_i\, \epsilon_j^k\,, \tag{29}$$

where the index k runs over all presynaptic spikes that occurred at time t_i.

This sum can be calculated by introducing *modulation factors* S_j^m which obey the following iteration:

$$S_j^m \;=\; S_j^{m-1} \times \exp[-(t_j^m - t_j^{m-1})/\tau_p] \;+\; \epsilon_j^m\,. \tag{30}$$

The idea is to calculate Expression (29) for each spike by only updating the modulation factor obtained from the preceding spike. This is done by evaluating the expression $S_j^m\; P(t_i - t_j^m)\; \epsilon_i$. Since $P(t) \;=\; A_p\; \exp[-t/\tau_p]$, we can expand this expression as follows:

$$\begin{aligned} S_j^m\; P(t_i - t_j^m)\; \epsilon_i \;&=\; \left[S_j^{m-1}\; \exp[-(t_j^m - t_j^{m-1})/\tau_p] + \epsilon_j^m\right] \\ &\quad \times A_p\; \exp[-(t_i - t_j^m)/\tau_p]\; \epsilon_i \\ &= S_j^{m-1}\; P(t_i - t_j^{m-1})\; \epsilon_i \\ &\quad + P(t_i - t_j^m)\; \epsilon_i\; \epsilon_j^m \\ &= S_j^{m-2}\; P(t_i - t_j^{m-2})\; \epsilon_i \\ &\quad + P(t_i - t_j^{m-1})\; \epsilon_i\; \epsilon_j^{m-1} \\ &\quad + P(t_i - t_j^m)\; \epsilon_i\; \epsilon_j^m \\ &\cdots \\ &= \sum_{k=0}^{m} P[t_i - t_j^k]\; \epsilon_i\; \epsilon_j^k \end{aligned} \tag{31}$$

Similarly, LTD occurs at the time of each pre-synaptic spike t_j, and is determined by all pairs made by all post-synaptic spikes t_i^k that occurred at that time, which is given by:

$$\sum_{k=0}^{m} Q[t_j - t_i^k]\; \epsilon_i^k\; \epsilon_j\,. \tag{32}$$

This expression can also be calculated using modulation factors, by evaluating $S_i^m\; Q(t_i^m - t_j)\; \epsilon_j$ using the iteration

$$S_i^m \;=\; S_i^{m-1} \times \exp[-(t_i^m - t_i^{m-1})/\tau_q] \;+\; \epsilon_i^m\,. \tag{33}$$

Thus, at each time a spike occurs, either pre- or post-synaptically, all previous spikes can be taken into account by updating the corresponding modulation factor S_k. This enables us to calculate an all-to-all pairing scheme using a minimum of computations (the total number of exponentials to be calculated equals $1 + n_s$ at each post-synaptic spike, where n_s is the number of synapses, while only two exponentials must be calculated for each pre-synaptic spike). Note that this algorithm is exact.

Appendix 2: Steady-state synaptic weight

In this appendix, we provide expressions for the steady-state synaptic weight of the particular model studied here (for similar derivations, see Gütig et al. 2003; Burkitt et al. 2004).

To obtain the steady-state synaptic weight $\langle\omega_{ji}\rangle$, we start from Eq. 5, neglect the spike eligibility factors ($\epsilon_i = \epsilon_j = 1$), and take the limit of $t \to \infty$. In this limit, $\mathrm{d}\omega_{ji}/\mathrm{d}t \to 0$, which gives:

$$\bar{F}_{\mathrm{LTP}}\; (\langle\omega_{ji}\rangle - \omega_{\mathrm{LTP}}) + \bar{F}_{\mathrm{LTD}}\; (\langle\omega_{ji}\rangle - \omega_{\mathrm{LTD}}) = 0\,, \tag{34}$$

where $\bar{\mathrm{F}}_{\mathrm{LTP}} = \lim_{t\to\infty} \mathrm{F}_{\mathrm{LTP}}(t)$ and similarly for $\bar{F}_{\mathrm{LTD}} = \lim_{t\to\infty} \mathrm{F}_{\mathrm{LTD}}(t)$.

If we assume that $\omega_{\mathrm{LTD}} = 0$, we have the following:

$$\langle\, \omega_{ji} \,\rangle \;=\; \frac{\omega_{\mathrm{LTP}}}{1 + \frac{\bar{F}_{\mathrm{LTD}}}{\bar{F}_{\mathrm{LTP}}}}. \tag{35}$$

Thus, predicting the steady-state synaptic weight $\langle\omega_{\mathrm{ji}}\rangle$ amounts to calculate the term $\bar{\mathrm{F}}_{\mathrm{LTD}}/\bar{\mathrm{F}}_{\mathrm{LTP}}$. To calculate this term, we expand $\bar{\mathrm{F}}_{\mathrm{LTP}}$ as:

$$\bar{F}_{\mathrm{LTP}} = \lim_{t\to\infty} \sum_{t_i,t_j} P(t - t_j)\delta(t - t_i) \tag{36}$$

$$= \lim_{t\to\infty} \sum_{t_i,t_j} \left[\int_{-\infty}^{\infty} P(t - t')\delta(t' - t_j)\mathrm{d}t' \right] \delta(t - t_i). \tag{37}$$

Reorganizing the sums, we have the following:

$$\bar{F}_{\mathrm{LTP}} = \lim_{t\to\infty} \int_{-\infty}^{\infty} P(t - t') \left[\sum_{t_j} \delta(t' - t_j) \right] \times \left[\sum_{t_i} \delta(t - t_i) \right] \mathrm{d}t' \tag{38}$$

$$= \lim_{t\to\infty} \int_{-\infty}^{\infty} P(t - t')\; \rho_j(t')\; \rho_i(t)\; \mathrm{d}t' \,, \tag{39}$$

where $\rho_j(t) = \sum_{t_j} \delta(t - t_j)$ and $\rho_i(t) = \sum_{t_i} \delta(t - t_i)$ are the pre- and post-synaptic spike trains, respectively.

Following the change of variables $t' = t - \tau$, one can write this expression as:

$$\bar{F}_{\mathrm{LTP}} = \lim_{t\to\infty} \int_{-\infty}^{\infty} P(\tau)\; \rho_j(t - \tau)\; \rho_i(t)\; \mathrm{d}\tau \,. \tag{40}$$

The term $\rho_j(t-\tau)\,\rho_i(t)$ can be expressed as a function of the cross-correlation between pre- and post-synaptic spikes:

$$C_{ji}(\tau) = \lim_{t\to\infty} \frac{1}{N_{ji}} \left[\rho_j(t)\; \rho_i(t + \tau)\right] \tag{41}$$

$$= \lim_{t\to\infty} \frac{1}{N_{ji}} \left[\rho_j(t - \tau)\; \rho_i(t)\right] \,, \tag{42}$$

where $\frac{1}{N_{ji}}$ is a normalization factor. Inserting this relation into Eq. 40, we obtain the expression:

$$\bar{F}_{\mathrm{LTP}} = N_{ji} \int_{-\infty}^{\infty} P(\tau)\; C_{ji}(\tau)\; \mathrm{d}\tau \,, \tag{43}$$

and similarly for $\bar{\mathrm{F}}_{\mathrm{LTD}}$:

$$\bar{F}_{\mathrm{LTD}} = N_{ji} \int_{-\infty}^{\infty} Q(\tau)\; C_{ij}(\tau)\; \mathrm{d}\tau \,. \tag{44}$$

The steady-state synaptic weight is then given by:

$$\langle\, \omega_{ji} \,\rangle \;=\; \frac{\omega_{\mathrm{LTP}}}{1 + \frac{\int\, Q(\tau)\; C_{ij}(\tau)\; \mathrm{d}\tau}{\int\, P(\tau)\; C_{ji}(\tau)\; \mathrm{d}\tau}}. \tag{45}$$

In particular, when pre-synaptic and post-synaptic spikes are decorrelated by using surrogate postsynaptic trains (see text), $\mathrm{C_{ij}}(\tau) = \mathrm{C_{ji}}(\tau) = cst.$, and we have the following:

$$\langle\, \omega_{ji} \,\rangle \;=\; \frac{\omega_{\mathrm{LTP}}}{1 + \frac{A_q\; \tau_q}{A_p\; \tau_p}} \;=\; \frac{\omega_{\mathrm{LTP}}}{1 + (A_-/A_+)} \,, \tag{46}$$

where $A_+ = \mathrm{A_p}\;\tau_\mathrm{p}$ and $A_- = \mathrm{A_q}\;\tau_\mathrm{q}$ are the positive and negative areas under the STDP function, respectively.

Acknowledgements Research supported by the CNRS, ACI, HFSP and the European Community (FACETS).

References

Abarbanel HD, Gibb L, Huerta R, Rabinovich MI (2003) Biophysical model of synaptic plasticity dynamics. Biol Cybern 89:214–226

Abeles M (1991) Corticonics: neural circuits of the cerebral cortex. Cambridge University Press, Cambridge

Anwyl R (2006) Induction and expression mechanisms of postsynaptic NMDA receptor-independent homosynaptic long-term depression. Prog Neurobiol 78:17–37

Badoual M, Zou Q, Davison AP, Rudolph M, Bal T, Frégnac Y, Destexhe A (2006) Biophysical and phenomenological models of multiple spike interactions in spike-timing dependent plasticity. Int J Neural Syst 16:79–97

Bell CC, Han VZ, Sugawara Y, Grant K (1997) Synaptic plasticity in a cerebellum-like structure depends on temporal order. Nature 387:278–281

Bi GQ, Poo MM (1998) Synaptic modifications in cultured hippocampal neurons: dependence on spike timing, synaptic strength and postsynaptic cell type. J Neurosci 18:10464–10472

Burkitt AN, Meffin H, Grayden DB (2004) Spike-timing-dependent plasticity: the relationship to rate-based learning for models with weight dynamics determined by a stable fixed point. Neural Comput 16:885–940

Castellani GC, Quinlan EM, Cooper LN, Shouval HZ (2001) A biophysical model of bidirectional synaptic plasticity: dependence on ampa and nmda receptors. Proc Nat Acad Sci USA 98:12772–12777

de Charms RC, Merzenich MM (1996) Primary cortical representation of sounds by the coordination of action-potential timing. Nature 381:610–613

Dan Y, Poo MM (2006) Spike timing-dependent plasticity: from synapse to perception. Physiol Rev 86:1033–1048

Debanne D, Gahwiler BH, Thompson SM (1994) Asynchronous pre- and postsynaptic activity induces associative long-term depression in area CA1 of the rat hippocampus in vitro. Proc Natl Acad Sci USA 91:1148–1152

Destexhe A, Paré D (1999) Impact of network activity on the integrative properties of neocortical pyramidal neurons in vivo. J Neurophysiol 81:1531–1547

Destexhe A, Mainen ZF, Sejnowski TJ (1994) An efficient method for computing synaptic conductances based on a kinetic model of receptor binding. Neural Comput 6:10–14

Destexhe A, Mainen ZF, Sejnowski TJ (1998) Kinetic models of synaptic transmission. In: Methods in neuronal modeling, chapter 1, MIT Press, Cambridge, Massachusetts, pp 1–26

Destexhe A, Rudolph M, Fellous JM, Sejnowski TJ (2001) Fluctuating synaptic conductances recreate in-vivo-like activity in neocortical neurons. Neurosci 107:13–24

Destexhe A, Rudolph M, Paré D (2003) The high-conductance state of neocortical neurons in vivo. Nat Rev Neurosci 4:739–751

Duguid I, Sjostrom PJ (2006) Novel presynaptic mechanisms for coincidence detection in synaptic plasticity. Curr Opin Neurobiol 16:312–322

Froemke RC, Dan Y (2002) Spike timing-dependent synaptic modification induced by natural spike trains. Nature 416:433–438

Gerstner W, Kistler W (2002) Spiking neuron models. Cambridge University Press, Cambridge

Gerstner W, Kempter R, van Hemmen JL, Wagner H (1996) A neuronal learning rule for sub-millisecond temporal coding. Nature 383:76–81

Gütig R, Aharonov R, Rotter S, Sompolinsky H (2003) Learning input correlations through nonlinear temporally asymmetric Hebbian plasticity. J Neurosci 23:3697–3714

Hebb DO (1949) The organization of behavior. John Wesley & Sons, New York

Hines ML, Carnevale NT (1997) The neuron simulation environment. Neural Comput 9:1179–1209

Hodgkin AL, Huxley AF (1952) A quantitative description of membrane current and its application to conduction and excitation in nerve. J Physiol (Lond) 117:500–544

Izhikevich EM, Desai NS (2003) Relating STDP to BCM. Neural Comput 15:1511–1523

Karbowski J, Ermentrout GB (2002) Synchrony arising from a balanced synaptic plasticity in a network of heterogeneous neural oscillators. Phys Rev E 65:031902

Karmarkar UR, Buonomano DV (2002) A model of spike-timing dependent plasticity: one or two coincidence detectors? J Neurophysiol 88:507–513

Kistler WM, van Hemmen JL (2000) Modeling synaptic plasticity in conjuction with the timing of pre- and postsynaptic action potentials. Neural Comput 12:385–405

Levy WB, Steward O (1983) Temporal contiguity requirements for long-term associative potentiation/depression in hippocampus. Neurosci 8:791–797

Magee JC, Johnston DA (1997) A synaptically controlled, associative signal for hebbian plasticity in hippocampal neurons. Science 275:209–213

Markram H, Lübke J, Frotscher M, Sakmann B (1997) Regulation of synaptic efficacy by coincidence of postsynaptic APs and EPSPs. Science 275:213–215

Montgomery JM, Pavlidis P, Madison DV (2001) Pair recordings reveal all-silent synaptic connections and the postsynaptic expression of long-term potentiation. Neuron 29:691–701

Morrison A, Aertsen A and Diesmann M (2007) Spike-timing dependent plasticity in balanced random networks. Neural Comput (in press)

Nicoll RA (2003) Expression mechanisms underlying long-term potentiation: a postsynaptic view. Philos Trans R Soc Lond B 358: 721–726

Paré D, Shink E, Gaudreau H, Destexhe A, Lang E (1998) Impact of spontaneous synaptic activity on the resting properties of cat neocortical neurons in vivo. J Neurophysiol 79:1450–1460

Pfister JP, Gerstner W (2006) Triplets of spikes in a model of spike timing-dependent plasticity. J Neurosci 26:9673–9682

Riehle A, Grun S, Diesmann M, Aertsen A (1997) Spike synchronization and rate modulation differentially involved in motor cortical function. Science 278:1950–1953

Roche KW, Tingley WG, Huganir RL (1994) Glutamate receptor phosphorylation and synaptic plasticity. Curr Opin Neurobiol 4:383–388

van Rossum MC, Bi GQ, Turrigiano GG (2000) Stable Hebbian learning from spike timing-dependent plasticity. J Neurosci 20:2211–2221

Rubin J, Lee DD, Sompolinsky H (2001) Equilibrium properties of temporally asymmetric Hebbian plasticity. Phys Rev Lett 86:364–367

Rubin JE, Gerkin RC, Bi G-Q, Chow CC (2005) Calcium time course as a signal for spike-timing-dependent plasticity. J Neurophysiol 93:2600–2613

Rudolph M, Destexhe A (2001) Do neocortical pyramidal neurons display stochastic resonance? J Comput Neurosci 11:19–42

Senn W, Markram H, Tsodyks M (2001) An algorithm for modifying neurotransmitter release probability based on pre- and postsynaptic spike timing. Neural Comput 13:35–67

Shouval HZ, Kalantzis G (2005) Stochastic properties of synaptic transmission affect the shape of spike time-dependent plasticity curves. J Neurophysiol 93:1069–1073

Shouval HZ, Bear MF, Cooper LN (2002) A unified model of nmda receptor-dependent bidirectional synaptic plasticity. Proc Nat Acad Sci USA 99:10831–10836

Sjöström J, Turrigiano GG, Nelson SB (2001) Rate, timing, and cooperativity jointly determine cortical synaptic plasticity. Neuron 32:1149–1164

Soderling TR, Derkach VA (2000) Postsynaptic protein phosphorylation and LTP. Trends Neurosci 23:75–80

Song S, Abbott LF (2001) Cortical development and remapping through spike timing-dependent plasticity. Neuron 32:339–350

Song S, Miller KD, Abbott LF (2000) Competitive Hebbian learning through spike-timing dependent synaptic plasticity. Nat Neurosci 3:919–926

Steriade M, Timofeev I, Grenier F (2001) Natural waking and sleep states: a view from inside neocortical neurons. J Neurophysiol 85:1969–1985

Vaadia E, Haalman I, Abeles M, Bergman H, Prut Y, Slovin H, Aertsen A (1995) Dynamics of neuronal interactions in monkey cortex in relation to behavioural events. Nature 373:515–518

Wang JQ, Arora A, Yang L, Parelkar NK, Zhang G, Liu X, Choe ES, Mao L (2005) Phosphorylation of AMPA receptors: mechanisms and synaptic plasticity. Mol Neurobiol 32:237–249

Zohary E, Shadlen MN, Newsome WT (1994) Correlated neuronal discharge rate and its implications for psychophysical performance. Nature 370:140–143

Zou Q, Rudolph M, Roy N, Sanchez-Vives M, Contreras D, Destexhe A. Reconstructing synaptic background activity from conductance measurements in vivo. Neurocomputing 65:673–678